International Journal of Mechanical, Industrial and Aerospace Sciences
ISSN: 2517-9950
Vol:11, No:11, 2017

Studying the Dynamical Response of Nano-Microelectromechanical Devices for Nanomechanical Testing of Nanostructures

Mohammad Reza Zamani Kouhpanji

***Abstract*—**Characterizing the fatigue and fracture properties of nanostructures is one of the most challenging tasks in nanoscience and nanotechnology due to lack of a MEMS/NEMS device for generating uniform cyclic loadings at high frequencies. Here, the dynamic response of a recently proposed MEMS/NEMS device under different inputs signals is completely investigated. This MEMS/NEMS device is designed and modeled based on the electromagnetic force induced between paired parallel wires carrying electrical currents, known as Ampere's Force Law (AFL). Since this MEMS/NEMS device only uses two paired wires for actuation part and sensing part, it represents highly sensitive and linear response for nanostructures with any stiffness and shapes (single or arrays of nanowires, nanotubes, nanosheets or nanowalls). In addition to studying the maximum gains at different resonance frequencies of the MEMS/NEMS device, its dynamical responses are investigated for different inputs and nanostructure properties to demonstrate the capability, usability, and reliability of the device for wide range of nanostructures. This MEMS/NEMS device can be readily integrated into SEM/TEM instruments to provide real time study of the fatigue and fracture properties of nanostructures as well as their softening or hardening behaviors, and initiation and/or propagation of nanocracks in them.

***Keywords*—**Ampere's force law, dynamical response, fatigue and fracture characterization, paired wire actuators and sensors, MEMS/NEMS devices.

I. Introduction

THE boundless benefits of the size-dependency and quantum effects of nanostructured materials, such as nanowires, nanotubes and nanosheets, became a driving force guiding the future technologies toward smaller and smaller dimensions [1]-[7]. This driving force made the nanotechnologies at the central focus in all research fields in all over the world. The mechanical properties of these nanostructured materials require to be precisely determined before being implemented into any nanodevices, such as electronic, nanophotonic and nanophononic devices. The mechanical performance of these nanodevices plays a critical role in the quantum efficiency of these nanodevices [8], [9]. That is why, in addition to the partial fractures during the fabrication processes as well as the strains/stresses induced by lattice mismatch between the nanodevices and their substrates, these nanodevices are repeatedly under the cyclic thermal loadings induced by thermal stresses/strains as a result of the heat lost in the nanodevices. These cyclic strains/stresses significantly reduce the quantum efficiency of the nanodevices by making nonhomogeneous distributions of the carriers and reducing the mobilities of the carriers in the active region [9]-[11].

Regardless of numerous well-established experimental techniques for understanding the mechanical properties of the nanostructures under static loadings [12]-[18], there are a few attempts in understanding the mechanical properties of the nanostructures under cyclic loadings. The main drawback for studying the mechanical properties of the nanostructures under cycling loadings (also named fatigue and fracture properties) is the designing of a microelectromechanical device (NEMS/MEMS device) with fast and linear dynamical response at high frequencies. To the best knowledge of the author, there are only three different proposed NEMS/MEMS devices for fatigue and fracture characterization of the nanostructures [19]-[222]. These NEMS/MEMS devices can be categorized into three categories, as electrostatic NEMS/MEMS devices, electrothermal NEMS/MEMS devices, and piezoelectric NEMS/MEMS devices.

One cannot apply large current/voltage to the electrostatic-based MEMS/NEMS devices because the large electrostatic forces between the substrate and the combs cause the bending of the combs and failure of the device [23], [24]. Consequently, the electrostatic-based MEMS/NEMS devices usually produce less force in contrast to other MEMS/NEMS devices, such as electrothermal-based MEMS/NEMS devices [22], [25]. However, an alternative is to increase the number of the combs or to design a complex flexible structure for generating large displacements/forces which cause the nonlinear dynamical response of the electrostatic NEMS/MEMS devices. In contrast to the electrostatic actuators, the electrothermal can generate large displacements in the costs of high power consumptions and highly nonlinear dynamical behaviors due to the coupled thermal-mechanical effects [26], [27]. Similarly, the piezoelectric NEMS/MEMS devices behave a very nonlinear response due to coupled electrical-mechanical effects. The nonlinear behavior of all NEMS/MEMS devices is the main reason for the lack of information about the fatigue and fracture properties of the nanostructures.

To eliminate this lack of knowledge, a new NEMS/MEMS device for fatigue and fracture characterizing the nanostructures was proposed by this author [28]. In this NEMS/MEMS device (called PWCC device), two paired

Mohammad Reza Zamani Kouhpanji is with the Electrical and Computer Engineering Department, University of Minnesota Twin Cities, Minneapolis, MN 55455, USA (phone: +1(618) 305-9636, e-mail: zaman022@umn.edu).

wires carrying currents are used to generate sufficient static and dynamic loadings as well as their combinations for fatigue and fracture characterization of the nanostructures. The currents passing through the paired wires induce a magnetic force on the wires according to the Amperes' force law. Designing the actuator part and sensor part of the PWCC devices using the AFL results in a very simple and cost-effective NEMS/MEMS device with low power consumption and high sensitivity appropriate for fatigue and fracture characterization of the nanostructures.

The previous works on the PWCC devices, [22], [23], mainly focused on the designing the PWCC devices with considering the practical limitations in addition to analyzing the sensitivity of these devices. However, since the main application of the PWCC devices is generating cyclic loadings at high frequencies, the dynamical response of them plays a significant role on the performance of the PWCC devices and their capability for fatigue and fracture characterizing of the nanostructures. Therefore, here the dynamical response of the PWCC devices is comprehensively studied for different input signals. Furthermore, the effects of the mechanical properties of the nanostructures on the dynamical response of the PWCC devices are investigated as well.

II. Modeling

A schematic view of the PWCC devices is provided in Fig. 1. The magnetic field generated by the parallel wires I and II produces an attractive or repulsive force applying on the wires I and II, therefore the wires I and II are the only two parts making the actuation part of the PWCC devices. The wire II is connected to the wire III by the nanostructure as shown in Fig. 1. The nanostructure, which can be a single or arrays of nanowires, nanotubes or even a patterned thin film or nanosheet, causes the wire III to vibrate. The vibration of the wire III can be sensed as an oscillating signal in the wire IV, therefore the wires III and IV are the only two parts making the sensor part of the PWCC device. It should be mentioned that, in order to sense a signal at the wire IV, at least one of the wires III or IV must have a DC current.

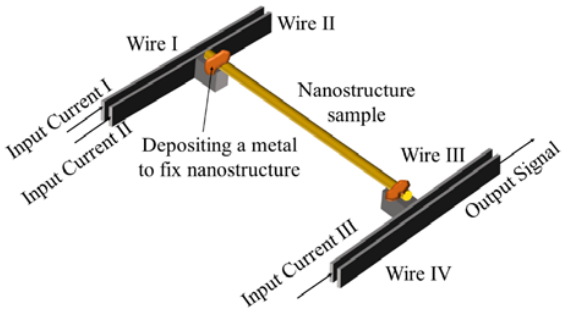

Fig. 1 A schematic view of the PWCC device. The nanostructure is shown to be a single nanowire which can be an array of nanowires/nanotubes or thin films, nanosheets/nanowalls

The cross-sections of the wires I and II are shown in Fig. 2. The cross-sections are considered rectangular shape to be compatible with the photolithography processes. The wires are considered along the y-axis in the z-y plane, and the origin on of the coordinate system is placed at the center of the wire I.

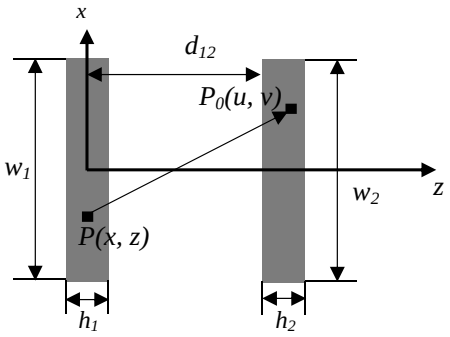

Fig. 2 The cross-section of the wires I and II making the actuator part of the PWCC devices. Note that the sensor part of the PWCC devices (wires III and IV) has the same configurations

The cross-section dimensions of the wires and the distance between them are considered very smaller than the wires lengths, hence the side-effects are negligible. Neglecting the side-effects is equivalent with the zero-magnetic field in y-direction. Furthermore, even though the magnetic field in z-direction is not zero, it does not apply any force on the wire II due to the symmetry [21], [22]. Consequently, the only nonzero magnetic field component induced by each element of the wire I, say point $P(x, z)$, at each element of the wire II, say point $P_0(u, v)$, can be determined as follows

$$H_x(u,v) = \frac{2i_1}{cS_1} \int_{-h_1/2}^{h_1/2} \int_{-w_1/2}^{w_1/2} \frac{v-z}{(u-x)^2+(v-z)^2} dxdz \tag{1}$$

where w_1 is the depth of the wire I; h_1 is the width of the wire I; S_1 is the cross-section area of the wire I; i_1 is the current passing in the wire I; and c is the light speed in the space. The results of the integrals in (1) are provided in [22], which can be used to determine the total force exerted on the wire II in z-direction

$$F_z = -\mu_0 L_2 \frac{i_2}{S_2} \int_{d_{12}}^{d_{12}+h_2} \int_{-w_2/2}^{w_2/2} H_x(u,v) dudv \tag{2}$$

where i_2 is the current passing in the wire II; S_2 is the cross-section of the wire II; d_{12} is the distance between the center of the wire I to the left edge of the wire II; w_2 is the depth of the wire II; h_2 is the width of the wire II; and L_2 is the length of the wire II. Consequently, the transfer function of the actuator part in the Laplace space can be determined as

$$TF_{Actuator} \equiv \frac{F(s)}{I_{I-II}(s)} = -\mu_0 \frac{2L_2}{cS_1S_2} \int_{d_{12}}^{d_{12}+h_2} \int_{-w_2/2}^{w_2/2} \int_{-h_1/2}^{h_1/2} \int_{-w_1/2}^{w_1/2} \frac{v-z}{(u-x)^2+(u-z)^2} dxdzdudv \quad (3)$$

where, $I_{I-II}(s)$ is the Laplace transfer of the product of the i_1 and i_2 currents; and F is the Laplace transfer of the F_z.

Since the nanostructures have much smaller dimensions comparing to the other parts of the NEMS/MEMS devices, their mass is much smaller than the mass of the other parts. Therefore, ignoring the mass of the nanostructure, the whole PWCC devices can be readily modeled by two masses, wires II and III, connected to each other by a spring and damper, as it is shown in Fig. 3. The dynamic equation of motions of the PWCC devices in the Laplace space can be written as

$$\begin{cases} \left(M_2 s^2 + (\lambda_2 + \lambda_n)s + K_2 + K_n\right) X_{II}(s) - (\lambda_n s + K_n) X_{III}(s) = F(s) \\ -(\lambda_n s + K_n) X_{II}(s) + \left(M_3 s^2 + (\lambda_3 + \lambda_n)s + K_3 + K_n\right) X_{III}(s) = 0 \end{cases} \quad (4)$$

where, $X_{II}(s)$ is the Laplace transfer of the wire II displacement; $X_{III}(s)$ is the Laplace transfer of the wire III displacement; M_2 is the mass of the wire II; M_3 is the mass of the wire III; K_2 is the spring constant of the wire II; K_3 is the spring constant of the wire III; λ_2 is the damping coefficient of the wire II; λ_3 is the damping coefficient of the wire III; K_n is the spring constant of the nanostructure; and λ_n is the damping coefficients of the nanostructure.

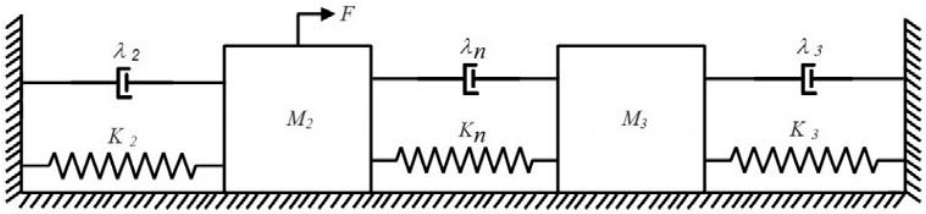

Fig. 3 Dynamical modeling of the PWCC device's structure

The spring constants of the wires and the nanostructure are related to their dimensions and their mechanical properties as

$$K_2 = \frac{384E_2I_2}{L_2^3}, \quad K_3 = \frac{192E_3I_3}{L_3^3}, \quad K_n = \frac{E_nS_n}{L_n} \quad (5)$$

where, E_j $(j=2,3,n)$ are the Young's modulus of the wires; L_j $(j=2,3,n)$ are the length of the wires and the nanostructure; I_j $(j=2,3)$ are the second moments of the area of the wires; and S_n is the cross-section of the nanostructure. Since the velocity of the wire III contributes on the signal detected at the sensor part of the PWCC device, the transfer function of the wire III velocity is derived at (6), where $V_{III}(s)$ is the velocity of the wire III in the Laplacian space.

$$TF_{III} \equiv \frac{V_{III}(s)}{F(s)} = \frac{(\lambda_n s + K_n)s}{\left(M_2 s^2 + (\lambda_2 + \lambda_n)s + K_2 + K_n\right)\left(M_3 s^2 + (\lambda_3 + \lambda_n)s + K_3 + K_n\right) - (\lambda_n s + K_n)(\lambda_n s + K_n)} \quad (6)$$

It should be emphasized that, according to [28], [29], the displacement of each point along wire III can be determined by multiplying its time response (which can be determined by conducting the Laplace inverses of transfer functions at (6)) and its eigenfunction. The eigenfunction of a continuous beam under fixed-fixed boundary condition, $\psi(y)$, is [28]

$$\psi(y) = \cosh\left(a_m \frac{y}{L_3}\right) - \cos\left(a_m \frac{y}{L_3}\right) - \frac{\cosh(a_m) - \cos(a_m)}{\sinh(a_m) - \sin(a_m)}\left(\sinh\left(a_m \frac{y}{L_3}\right) - \sin\left(a_m \frac{y}{L_3}\right)\right) \quad (7)$$

Here, a_m corresponds to the mode of resonant of the wire III, which are the solutions of $\cosh(a_m)\cos(a_m)=1$.

The last step of analyzing the dynamical response of the PWCC devices is to determine the transfer function of the sensing part. As it was mentioned earlier, in order to detect a signal at the sensing part of the PWCC devices, at least one of the wires III or IV must carry a current. For simplicity and avoiding the power consumption of the PWCC device, it is assumed that the wire III carries a DC current, i_3. In this case, since the wire III's current generates a magnetic field around

the wire IV while it has a relative velocity with respect to the wire IV, the wire III motion induces a current in the wire IV which must be detected as the output of the PWCC device [30]. The transfer function of the sensing part can be written as follows

$$TF_{Sensor} \equiv \frac{\Delta V_{IV}}{V_{III}} = \frac{i_3}{\psi\left(\frac{L_4}{2}\right) S_4} \int_0^{L_4} \psi(y)dy \int_0^{h_4} \int_{-w_4/2}^{w_4/2} H_x dx_0 dz_0 \quad (8)$$

where, V_{III} is the Laplace transfer of the wire III velocity; ΔV_{IV} is the Laplace of the induced voltage between the two ends of the wire IV; S_4 is the cross-section area of the wire IV; and $\psi(L_4/2)$ is the value of the eigenfunction at the center of the wire IV.

It should be mentioned that the PWCC device can generate both cyclic and static loadings depending on the wires I and II currents type. For the case of the static loadings, both wires I and II must have DC currents. However, for the case of cyclic loadings, at least one of the wires I or II must have an AC current, while the another one can be either DC or AC current. In the latter case, one may design an electrical circuit in order to pick the desired frequency and filter the remains. Therefore, it may be necessary to associate the PWCC device with an amplifier and/or filter circuit. Here, for simplicity, a common state variable circuit is considered. The state variable circuits' cut-off frequency and gain can be tuned independently while keeping its Q-factor very large and narrow [31]. These unique features make the state variable circuits suitable for PWCC devices. The transfer function of a state variable circuit can be written as [22], [31]

$$TF_{Circuit} \equiv \frac{\Delta V_{Circuit}}{\Delta V_{IV}} = \frac{a_0 s}{s^2 + a_1 s + a_2}$$
$$a_0 = \frac{R_8 R_6}{R_7 R_5} \frac{1}{R_1 C_1} \frac{1 + R_4/R_3}{1 + R_6/R_5}, \quad a_1 = \frac{1}{R_1 C_1} \frac{1 + R_4/R_3}{1 + R_6/R_5}, \quad (9)$$
$$a_2 = \frac{R_4}{R_3} \frac{1}{R_1 C_1 R_2 C_2}$$

where, R_i $(i=1,2,...,8)$ are resistors; C_i $(i=1,2)$ are capacitors; ΔV_{IV} is the induced voltage at the wire IV; $\Delta V_{Circuit}$ is the output signal of the state variable circuit operating at its bandpass mode.

III. Results

The total transfer function of the PWCC device is determined by the product of the all transfer functions as

$$TF(s) \equiv \frac{\Delta V_{Circuit}}{I_{I-II}} = TF_{Actuator} \times TF_{III} \times TF_{Sensor} \times TF_{Circuit} \quad (10)$$

The first important dynamical parameters for any MEMS/NEMS device are the phase shift and gain in terms of input signal frequency. Fig. 4 depicts the total gain and phase shift of the PWCC device. The circuit elements of the state variable circuit, R_i and C_i, are chosen to have the same resonance frequency as the structure of the PWCC device. That is why the gain has a very small nonzero curvature at the resonance frequency even though the system is at the critical damping condition.

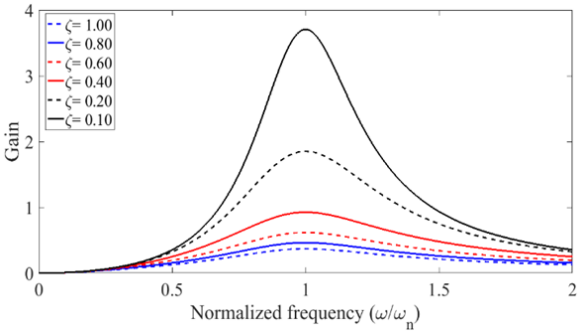

(a) The total gain of the PWCC device

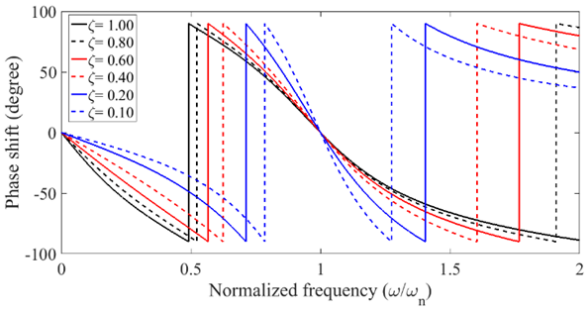

(b) The total phase shift of the PWCC device

Fig. 4 Total gain and phase shift of the PWCC device vs. the frequency normalized with respect to the 1st resonance frequency of the whole device for different mechanical damping ratios

As the damping increases, the maximum gain decreases. The phase shift at the first resonance frequency is zero for all damping ratios. Furthermore, the phase shift has higher dependency on the frequency around the resonance frequency when the damping is very small, and it behaves almost linear for larger damping values. Increasing the damping ratio reduces the PWCC device sensitivity, which is equivalent with a larger phase delay. This phase delay causes phase jumps (discontinuities of the phase shift) to happen at frequencies farther away from the resonance frequency.

In the following, the effects of the stiffness of the nanostructure on the dynamical response of the PWCC device are inspected, which is the most important parameters for an efficient design. Fig. 5 shows the resonance frequencies of the PWCC device and its maximum gain in terms of the nanostructure stiffness. In this configuration of the PWCC device, implementing a state variable circuit resulted the

PWCC device to have three resonance frequencies, in which two of them associated with the structure of the PWCC device and another one is associated with the circuit. Since the circuit is arbitrary and may be replaced with a more advanced circuit, its resonance frequency is not considered in evaluating the dynamical response of the PWCC device. One of the most crucial features of the PWCC devices is that the first resonance frequency slightly changes with respect to the nanostructure material or stiffness, which means that an initial design of the PWCC device is good enough for a wide range of nanostructures. Furthermore, Fig. 5 indicates that the maximum gain of the PWCC device does not degenerate for a wide range of the nanostructures if the PWCC device is designed to work around the 1st resonance frequency of the PWCC device rather than its 2nd resonance frequency.

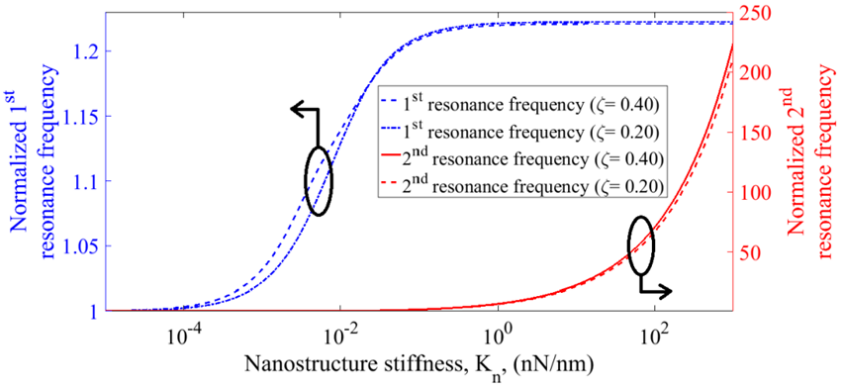

(a) Resonance frequencies of the PWCC device normalized with respect to their resonance frequencies at $K_n = 0$

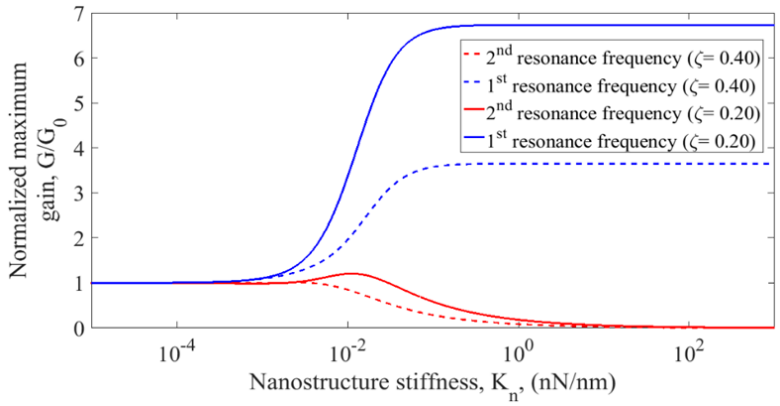

(b) The maximum gains normalized with respect to their maximum gains at $K_n = 0$ (G_0)

Fig. 5 Investigating the effects of the nanomaterials stiffness on the resonance frequencies, (a), and the maximum gain, (b), of the PWCC device

As it was already mentioned, the dynamical response of the PWCC device, or even any NEMS/MEMS devices, is the critical factor for successfully conducting fatigue and fracture experiments of the nanostructures. A successful design requires a linear, fast, and stable dynamical response of the NEMS/MEMS device for different input signals, such as pulsed, step or sinusoidal, at high frequencies. Fig. 6 shows the time response of the PWCC device under pulsed and step input signals, Fig. 6 (a), as well as square and sinusoidal input signals, Fig. 6 (b). The PWCC device provides a linear and stable time response for all input signals, which is an evidence for the capability of the PWCC device for fatigue and fracture experiments of the wide ranges of the nanostructures.

IV. Conclusion

This work investigates the dynamical response of the PWCC devices. The dynamical responses, gain and phase shift, of the PWCC device were examined for different physical parameters. Variation of the nanostructures stiffness slightly impacts the first resonance frequency of the PWCC device, which means that the device can be designed to work for a wide range of nanostructure samples. The maximum gain of the PWCC device at the first resonance frequency increases as the stiffness of the nanostructure increases, while it behaves reversely at the second resonance frequency. This behavior of the PWCC device proposes the importance of designing the PWCC device at the first resonance frequency. Furthermore, the dynamical analysis of the PWCC device for different input

signals highlights the linear, fast, and stable dynamical response for the PWCC device, which are the most crucial features of a successful design of NEMS/MEMS device for fatigue and fracture experiments of nanostructures.

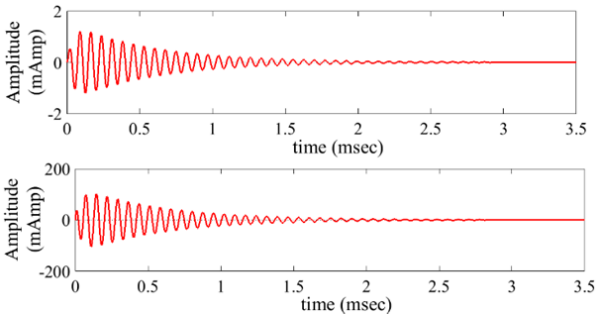

(a) top plot is the response for a step input signal, bottom plot is the response for a pulse input signal

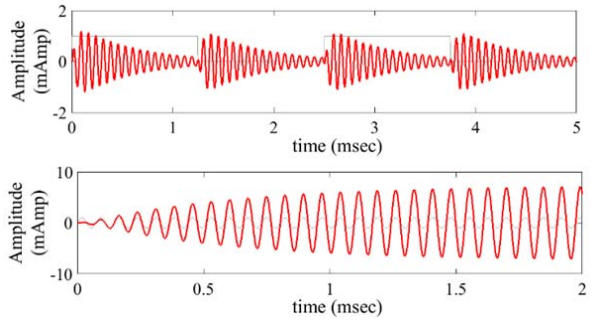

(b) top plot is the response for a square input signal, bottom plot is the response for a sinusoidal input signal at frequency equal to the 1st resonance frequency of the PWCC device

Fig. 6 Dynamical response of the PWCC device for different input signals, $I_{I\text{-}II}$. The narrow gray lines in the (b) shows the input signal

REFERENCES

[1] Mohammadi R, Shahrokhian S. In-situ fabrication of nanosheet arrays on copper foil as a new substrate for binder-free high-performance electrochemical supercapacitors. Journal of Electroanalytical Chemistry. 2017 Oct 1; 802:48-56.

[2] Ozel T, Zhang B, Gao R, Day RW, Lieber CM, Nocera DG. Electrochemical Deposition of Conformal and Functional Layers on High Aspect Ratio Silicon Micro/Nanowires. Nano Letters. 2017 Jun 16.

[3] Yan H, Hohman JN, Li FH, Jia C, Solis-Ibarra D, Wu B, Dahl JE, Carlson RM, Tkachenko BA, Fokin AA, Schreiner PR. Hybrid metal-organic chalcogenide nanowires with electrically conductive inorganic core through diamondoid-directed assembly. Nature materials. 2017 Mar 1; 16(3):349-55.

[4] Lupan O, Postica V, Wolff N, Polonskyi O, Duppel V, Kaidas V, Lazari E, Ababii N, Faupel F, Kienle L, Adelung R. Localized Synthesis of Iron Oxide Nanowires and Fabrication of High Performance Nanosensors Based on a Single Fe2O3 Nanowire. Small. 2017 Apr 1; 13(16).

[5] Han D, Jing X, Wang J, Ding Y, Cheng Z, Dang H, Xu P. Three-dimensional Co 3 O 4 Nanowire@ NiO Nanosheet Core-shell Construction Arrays as Electrodes for Low Charge Transfer Resistance. Electrochimica Acta. 2017 Jul 1; 241:220-8.

[6] Zhao Y, Chang C, Teng F, Zhao Y, Chen G, Shi R, Waterhouse GI, Huang W, Zhang T. Water Splitting: Defect-Engineered Ultrathin δ-MnO2 Nanosheet Arrays as Bifunctional Electrodes for Efficient Overall Water Splitting (Adv. Energy Mater. 18/2017). Advanced Energy Materials. 2017 Sep 1; 7(18).

[7] Zhou L, Shao M, Zhang C, Zhao J, He S, Rao D, Wei M, Evans DG, Duan X. Hierarchical CoNi-Sulfide Nanosheet Arrays Derived from Layered Double Hydroxides toward Efficient Hydrazine Electrooxidation. Advanced Materials. 2017 Feb 1; 29(6).

[8] Zamani Kouhpanji, MR. Investigating the classical and non-classical mechanical properties of GaN nanowires. MS Thesis, University of New Mexico, 2017, http://digitalrepository.unm.edu/ece_etds/354.

[9] Zamani Kouhpanji MR, Jafaraghaei U. A semianalytical approach for determining the nonclassical mechanical properties of materials. arXiv preprint arXiv:1706.06559. 2017 Jun 20.

[10] Bao W, Su Z, Zheng C, Ning J, Xu S. Carrier localization effects in InGaN/GaN multiple-quantum-wells LED nanowires: luminescence quantum efficiency improvement and "negative" thermal activation energy. Scientific reports. 2016; 6.

[11] Farsad E, Abbasi SP, Goodarzi A, Zabihi MS. Experimental parametric investigation of temperature effects on 60W-QCW diode laser. World Acad. Sci. Eng. Technol. 2011 Nov 28; 59: 1190-6.

[12] Huang JY, Zheng H, Mao SX, Li Q, Wang GT. In situ nanomechanics of GaN nanowires. Nano letters. 2011 Mar 18; 11(4):1618-22.

[13] Hung SC, Su YK, Fang TH, Chang SJ, Ji LW. Buckling instabilities in GaN nanotubes under uniaxial compression. Nanotechnology. 2005 Aug 16; 16(10):2203.

[14] Brown JJ, Baca AI, Bertness KA, Dikin DA, Ruoff RS, Bright VM. Tensile measurement of single crystal gallium nitride nanowires on MEMS test stages. Sensors and Actuators A: Physical. 2011 Apr 30; 166(2):177-86.

[15] Dai S, Zhao J, He MR, Wang X, Wan J, Shan Z, Zhu J. Elastic properties of GaN nanowires: Revealing the influence of planar defects on Young's modulus at nanoscale. Nano letters. 2014 Dec 4; 15(1):8-15.

[16] Nam CY, Jaroenapibal P, Tham D, Luzzi DE, Evoy S, Fischer JE. Diameter-dependent electromechanical properties of GaN nanowires. Nano letters. 2006 Feb 8; 6(2):153-8.

[17] Davydov VY, Averkiev NS, Goncharuk IN, Nelson DK, Nikitina IP, Polkovnikov AS, Smirnov AN, Jacobson MA, Semchinova OK. Raman and photoluminescence studies of biaxial strain in GaN epitaxial layers grown on 6H–SiC. Journal of applied physics. 1997 Nov 15; 82(10):5097-102.

[18] Moram MA, Barber ZH, Humphreys CJ. Accurate experimental determination of the Poisson's ratio of GaN using high-resolution x-ray diffraction. Journal of applied physics. 2007 Jul 15; 102(2):023505.

[19] Kahn H, Ballarini R, Mullen RL, Heuer AH. Electrostatically actuated failure of microfabricated polysilicon fracture mechanics specimens. InProceedings of the royal society of london a: mathematical, physical and engineering sciences 1999 Oct 8 (Vol. 455, No. 1990, pp. 3807-3823). The Royal Society.

[20] Hosseinian E, Pierron ON. Quantitative in situ TEM tensile fatigue testing on nanocrystalline metallic ultrathin films. Nanoscale. 2013 Nov 22; 5(24):12532-41.

[21] M. R. Zamani Kouhpanji, "Paired-wire carrying current actuators and piezoelectric beam sensors for microelectromechanical systems," Microsyst. Technol., p. MITE-D-17-00647, 2017.

[22] M. Reza and Z. Kouhpanji, "Designing and Analyzing Sensor and Actuator of a Nano / Micro-System for Fatigue and Fracture Characterization of Nanomaterials," vol. 11, no. 10, pp. 1649–1657, 2017.

[23] Pisano AP, Cho YH. Mechanical design issues in laterally-driven microstructures. Sensors and Actuators A: Physical. 1990 Apr 1; 23(1-3):1060-4.

[24] Legtenberg R, Groeneveld AW, Elwenspoek M. Comb-drive actuators for large displacements. Journal of Micromechanics and microengineering. 1996 Sep; 6(3):320.

[25] Maloney JM, Schreiber DS, DeVoe DL. Large-force electrothermal linear micromotors. Journal of Micromechanics and Microengineering. 2003 Nov 17; 14(2):226.

[26] Zhu Y, Corigliano A, Espinosa HD. A thermal actuator for nanoscale in situ microscopy testing: design and characterization. Journal of micromechanics and microengineering. 2006 Jan 5; 16(2):242.

[27] Que L, Park JS, Gianchandani YB. Bent-beam electro-thermal actuators for high force applications. InMicro Electro Mechanical Systems, 1999. MEMS'99. Twelfth IEEE International Conference on 1999 Jan 21 (pp. 31-36). IEEE.

[28] Kahrobaiyan MH, Asghari M, Hoore M, Ahmadian MT. Nonlinear size-dependent forced vibrational behavior of microbeams based on a non-classical continuum theory. Journal of Vibration and Control. 2012 Apr; 18(5):696-711.

[29] Nayfeh AH, Mook DT. Nonlinear oscillations. John Wiley & Sons; 2008 Sep 26.
[30] Nayfeh MH, Brussel MK. Electricity and magnetism. Courier Dover Publications; 2015 Feb 9.
[31] Taylor FJ. State Variable Filter Models. Digital Filters: Principles and Applications with MATLAB.: 183-96.